

Femtosecond laser writing of depressed cladding waveguides in sapphire

Sarah Winkler^{1,2}, Joachim R. Krenn², Jakob Wahl^{1,3}, Alexander Zesar^{1,2}, Yves Colombe¹, Klemens Schüppert¹, Clemens Rössler¹, Christian Sommer⁴, Philipp Hurdax⁴, Philip Lichtenegger⁴, and Bernhard Lamprecht⁴

¹Infineon Technologies Austria AG, Siemensstraße 2, A-9500 Villach, Austria

²Institut für Physik, Universität Graz, 8010 Graz, Austria

³Institut für Experimentalphysik, Universität Innsbruck, 6020 Innsbruck, Austria

⁴MATERIALS – Institute for Sensors, Photonics and Manufacturing Technologies, JOANNEUM RESEARCH, Franz-Pichler-Straße 30, 8160 Weiz, Austria

July 2023

1 Abstract

A promising solution for scalable integrated optics of trapped-ion quantum processors are curved waveguides guiding visible light within sapphire bulk material. To the best of our knowledge, no curved waveguides were investigated in sapphire so far and no waveguides for visible light in undoped planar sapphire substrates were reported. Here, we demonstrate femtosecond laser writing of depressed cladding waveguides in sapphire. Laser parameters such as pulse energy, pulse duration, and repetition rate, as well as waveguide geometry parameters were optimized to guide 728 nm light. This resulted in single-mode waveguides with a propagation loss of 1.9 (3) dB/cm. The investigation of curved waveguides showed a sharp increase in total loss for curvature radii below 15 mm. Our results demonstrate the potential of femtosecond laser writing as a powerful technique for creating integrated optical waveguides in the volume of sapphire substrates. Such waveguides could be a building block for integrated optics in trapped ion quantum processors.

2 Motivation

In trapped ion quantum computing, simulation, communication, and sensing, ions are the elementary building blocks for quantum information processing and high-precision measurements [1, 2, 3, 4]. Individual ions are confined by electromagnetic fields, and their internal (electronic) and motional states are manipulated with laser beams. Typically, free-space optics are used to perform quantum operations such as state preparation, readout, single-ion gates, and multi-ion entangling gates. However, this approach has significant drawbacks, such as beam instability, high cost, and limited scalability.

A promising alternative to overcome these drawbacks is the integration of waveguides into an ion trap [5, 6, 7]. In comparison to free-space optics, these approaches simplify the overall design of the quantum processing hardware and reduces the number of components that require regular alignment, thereby allowing for a stable system [8, 9]. Therefore, the integration of photonic components can be crucial to realize large-scale trapped ion quantum processors, where scalability and compactness are critical.

Femtosecond (fs) laser writing [10, 11] is a powerful technique to produce integrated optical waveguides in the volume of transparent substrates. In this process, a fs-laser beam is tightly focused in the substrate. While the substrate material is transparent for the wavelength of the fs laser, the high peak intensity at the laser focus allows for multiple photons to cross the bandgap simultaneously. This nonlinear photoionization or multi-photon absorption causes the beam to be absorbed in its focal area, generating a free electron plasma followed by energy transfer to the crystal lattice, leading to localized structural modifications [11]. Shifting the focal volume in 3D enables the fabrication of arbitrary structures with a high spatial resolution as set by the focal volume in the μm range.

Fs-laser writing can be used to create waveguides of different geometries and dimensions, including straight and bent waveguides, as well as waveguides with refractive index profiles that can be tailored to specific applications [12, 13]. The technique allows for the creation of complex optical circuits and devices [14]. The method is applicable to a wide range of transparent materials, including glass [15] and dielectric crystals [16, 17, 18, 19]. Importantly, fs-laser writing is a non-contact and non-destructive, maskless and rapid-prototyping technique, which allows for the creation of optical structures with high precision and reproducibility. Additionally, it can be integrated with other microfabrication techniques, such as FLICE (fs-laser irradiation and chemical etching) or fs-laser ablation to create complex optical structures on a single substrate [19].

In general, for fs-laser-modified volumes, three types of morphological changes are observed depending on laser parameters and material properties [11]. In the regime of low absorbed energy, smooth changes in the refractive index are created. The intermediate, medium absorbed energy regime leads to birefringent refractive index modifications. High energy modifications include the formation of empty voids due to micro explosions. Neither medium nor high energy modifications are desirable for optical guiding.

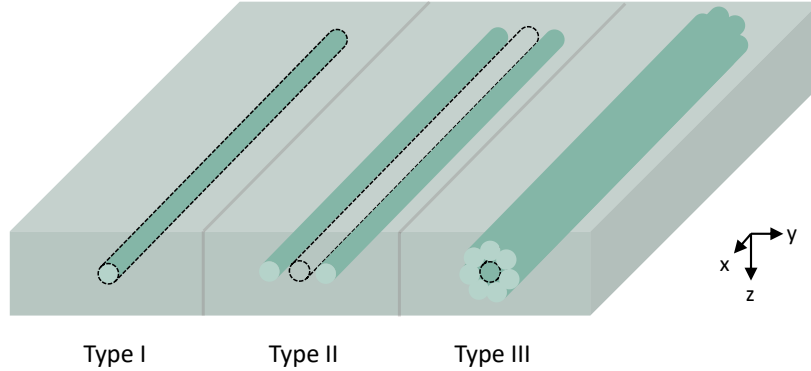


Figure 1: Types of fs-laser-written waveguides. Type I is made of a single fs-laser-written line (green area) which is congruent to the waveguide core (dotted area). Type II: Two parallel fs-laser-written lines enclose the waveguide core in between them. Type III consists of multiple lines surrounding the waveguide core. Adapted from [20].

Depending on the relative position of the waveguide core with respect to the fs-laser-written lines, three different types of waveguide configurations are defined [14]. Type I waveguides are based on a positive change in refractive index, allowing direct writing of waveguides as the irradiated focal volume acts as the waveguide core (Fig. 1 left). This type is common in glasses, but rarely met in crystals where the refractive index change is usually negative [19]. Type II waveguides are characterized by positive refractive index changes, which are located in the vicinity of the laser-written lines (Fig. 1 middle). For type II, the track has a lower index and cannot be used as a waveguide; however, the expansion of volume in the focal plane gives rise to a compression of its vicinity, leading to the refractive index increments in the surrounding of the track [19]. Usually, these waveguides are written in a dual-line geometry, where the waveguide core is located in between two laser-written lines. Type III waveguides are defined by negative refractive index changes as well, but significantly differ from the type II dual-line geometry. In type III waveguides, the unexposed waveguide core is surrounded by many low index lines close to each other acting as a low-index barrier that confines the guided light inside (Fig. 1 right). These waveguides are also referred to as depressed cladding waveguides (DCWs) [17, 15, 18] and this type of waveguide is explored in this article.

Sapphire is a material of choice for macroscopic and microfabricated ion traps [21, 22, 23, 24, 25] due to its low radio-frequency loss tangent and its high thermal conductivity compared to most dielectrics. These properties ensure that the trap temperature increases only minimally while applying radio-frequency voltages to the trap electrodes, which is desirable in particular for quantum

computing and sensing applications. Since sapphire is transparent to visible light due to its high bandgap of 8.7 eV, it is also a promising material for microfabricated, optical waveguides integrated into ion traps. Fs-laser modification of sapphire results in morphological changes in the crystal structure of the material due to the process of multi-photon absorption [16]. The intense light pulses cause a nonlinear interaction with the crystal lattice, leading to a localized modification of the sapphire. When the intensity of the laser pulses is high enough in the regime of low absorbed energy, the material in the focal volume is amorphized, which is a process where the crystal lattice structure of the material is destroyed. This amorphization process typically leads to a decrease in refractive index [19] and is the basis of the formation of a waveguide with a lower refractive index cladding surrounding unmodified sapphire material. It is important to note that, in general, besides amorphization, other mechanisms like localized crystalline lattice expansion in the focal volume and crystal lattice deformation can also cause a decrease of the refractive index [26].

Numerous articles on waveguides written in Ti-doped sapphire have been published [18, 27], as doped sapphire is a highly attractive laser material. In 2018, Bérubé et al. [17] reported the first waveguides in undoped sapphire substrates. Their waveguides were based on a depressed cladding structure and showed single mode behavior for 2850 nm and a propagation loss of 0.37 dB/cm. In April 2022, Wang et al. [28] reported the fabrication of a single-mode fiber Bragg grating in sapphire. In a preceding report, they described the successful fabrication of DCW in undoped sapphire and a total loss for a 1-cm long DCW of 6.09 - 6.68 dB (at 1550 nm), depending on the polarization direction of the in-coupling light. Also in April 2022, Kefer et al. [29] reported the fabrication of single mode waveguides in arbitrarily oriented, undoped sapphire crystals based on a photonic crystal approach achieving 1 dB/cm loss at 1550 nm. Thus, to the best of our knowledge, no curved waveguides were investigated in sapphire so far and no waveguides guiding visible light in undoped planar sapphire substrates were reported.

3 Methods

3.1 Femtosecond laser writing

We write the optical structures in sapphire using a Gaussian laser beam focused inside the bulk material. Moving the sample in 3D relative to the laser focus allows for precise creation of complex structures within the sapphire. The writing direction is perpendicular to the laser beam propagation direction, and the cross-section dimensions of the tracks of modified refractive index are determined by the diffraction-limited waist radius and the depth of focus of the laser beam, respectively. Fig. 2 shows a schematic drawing of the laser lithography system. The setup allows two laser beams to run collinearly with each other: a fs-laser beam for the multi-photon structuring process and a red HeNe laser for alignment. The laser platform allows the use of a wide range of focusing

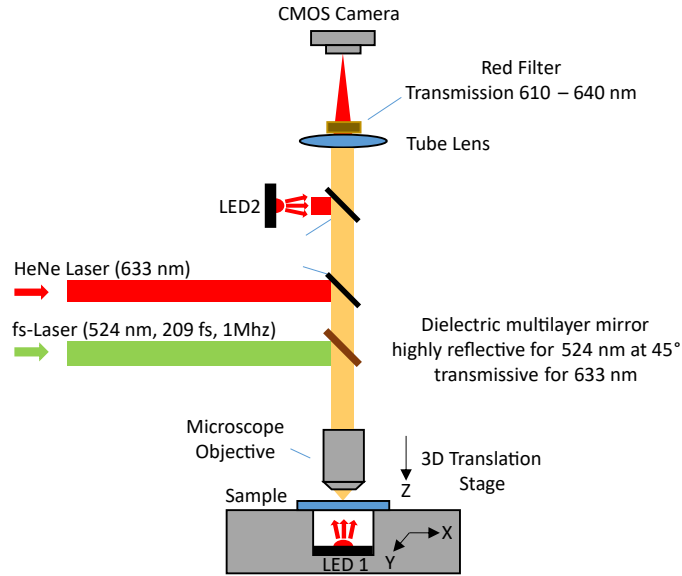


Figure 2: Optical setup of the laser lithography platform. A fs-laser is widened and collimated before it enters the setup. Here it is superimposed with a HeNe laser, which is visible in the imaging setup and used for z-levelling.-

optics with numerical apertures ranging from 0.25 to 1.4. Multi-photon structuring is performed with the second harmonic (524 nm) of a Spectra-Physics Spirit fs-laser at a pulse duration which can be set between 209 fs and 9 ps and a pulse repetition rate of maximum 1 MHz that can be divided down to single pulses. The fs-laser beam path includes an attenuator for external power control (half-wave plate and polarizing beam splitter), which is necessary to adjust the required maximum average power. Additionally, the average output power of the laser is adjusted via an external 0-5 V signal which allows for a fast adjustment of the power while laser writing. A beam expander before the optical setup shown in Fig. 2 ensures full and uniform illumination of the focusing objective. The polarization is adjustable from circular polarization to any linear polarization.

The structures written into the sapphire are obtained by moving the substrate in the horizontal xy-plane, which is perpendicular to the axis of the focusing optics (z-direction). The xy translation is obtained by a pair of linear motion stages (Newport XML210-S), with a minimum incremental movement of 1 nm, a typical bidirectional repeatability of ± 32 nm and a travel range of 210 mm. The writing setup shown in Fig. 2 is placed on a granite base to minimize the impact of external vibrations. The optical assembly (focusing optics and opto-mechanical components) is mounted on a breadboard which can be moved with a z-stage to shift the focus of the writing beam. The z-stage is a

high-load vertical linear stage from Newport (IMS100V) with a typical bidirectional repeatability of ± 150 nm and a vertical travel range of 100 mm for loads up to 400 N. Fine adjustment is achieved by an additional piezo z-stage on which the microscope objective is mounted. The linear stages are controlled by a Newport XPS-D motion controller.

An integrated inline video microscope with reflected and transmitted light illumination by means of a HeNe laser (633 nm) and two LEDs is used for focusing, leveling, alignment and real-time process monitoring. The HeNe-laser beam is used for focusing by imaging the reflected light from the optical interfaces of the sample onto the integrated camera. Correct adjustment of the focus of the writing beam is an important prerequisite for precise laser patterning. In addition, this method also makes it possible to align or level the sample horizontally via a tilt stage. This is necessary to remain parallel to the substrate surface when scanning over larger areas, meaning that the best possible focusing conditions are maintained even when scanning over centimeters. For process monitoring, the substrate is illuminated by a red LED underneath the transparent substrate. Since the laser exposure leads to a change in the optical properties of the structured areas (refractive index modification), the effect of laser structuring becomes visible in transmission light microscopy. The setup enables real-time monitoring of the laser patterning process and its quality. To prevent saturation of the camera with ambient light, filters are placed in front of the camera, which only transmit red light in the range of the LED and HeNe emission of approx. 610 to 640 nm.

An essential point of the experiment concerns the creation of so-called writing trajectories for the waveguide writing. We use a special operating mode of the Newport XPS motion controller, namely so-called PVT (Point-Velocity-Time) trajectories. In PVT, each individual path element is defined by the relative displacement (P), the final speed (V) and the duration for the path element (T) for all motion axes in the common motion group. An additional pass-through card for the Newport XPS motion controller (XPS-DRV00P) acts as a source for analog voltage signals. This card is configured together with the other motion axes (x-, y-, z-, z-Piezo) in a multi-axis motion group and delivers signals that are synchronized to the positions of the motion axes. The individual path elements for all involved motion axes are defined by the user in a text file, which is sent to the XPS controller. The controller then calculates and executes the trajectory by interpolating a smooth cubic function that traverses all specified positions at the defined times and velocities. Since a software for creating the PVT trajectory files is not commercially available, the necessary PVT files are generated by self-written Python scripts, implemented in Rhinoceros 3D (McNeel Europe), a 3D modeling software. Together with other important structuring parameters, such as laser writing velocity and the analog input for pulse energy, a text file is created which defines the PVT trajectory, required by the motion controller for movement in x-, y- and z-directions and for the laser power controlled by the analog signal.

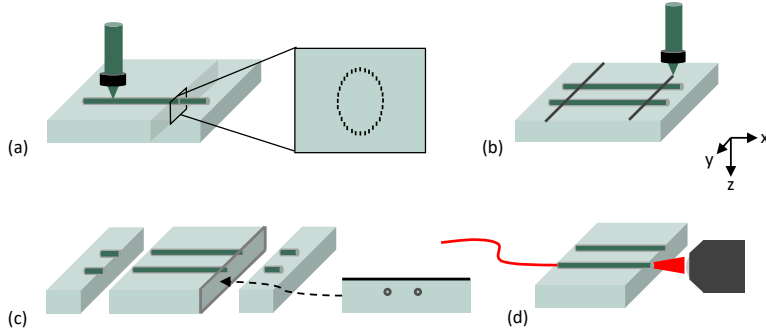


Figure 3: Schematic representation of 3D laser-writing of depressed cladding waveguides. (a) Constructing the DCW cladding with single scans arranged in a circle or ellipse (black dots in inset). Process repeated for multiple lines with different parameters, (b) laser ablation, (c) exposing end facets for further characterization via manual cleaving, (d) measurement setup for optical waveguide analysis.

3.2 Laser-writing of depressed cladding waveguides

A depressed cladding waveguide is constructed by scanning the sample with the fs-laser beam multiple times. As illustrated in Fig. 3(a), the cladding is built by offsetting the individual scans with respect to each other perpendicular to the writing direction to create a tubular arrangement of the tracks of reduced refractive index. The center of the pattern, here placed $200\ \mu\text{m}$ underneath the sample surface, is left unexposed, leading to the formation of the waveguide core surrounded by the built cladding with a lower refractive index.

For each set of experiments, multiple waveguides with different parameters were inscribed next to each other (Fig. 3(b)). Laser ablation and subsequent breaking was performed to create flat end facets of the waveguides for light in- and out-coupling. First, two laser ablation lines perpendicular to the waveguides were written on the surface of the sapphire sample using a high power setting of the laser and a repetition rate of $60\ \text{kHz}$ (Fig. 3(c)). Each sample was broken along the ablation lines into a $1\ \text{cm}$ -long piece by applying force in the negative z -direction at one side of the ablation line (Fig. 3(d)). The broken sidewalls were further prepared by grinding and polishing to achieve optical smoothness. The obtained cross-sections enable direct access to the DCW end facets (Fig. 3(c,d)).

3.3 Optical waveguides analysis

First, microscopic inspection of the waveguides, from above and also via the edges of the sapphire substrates, was performed. Afterwards, the mode profile as well as the losses of the waveguides were determined by optical characteriza-

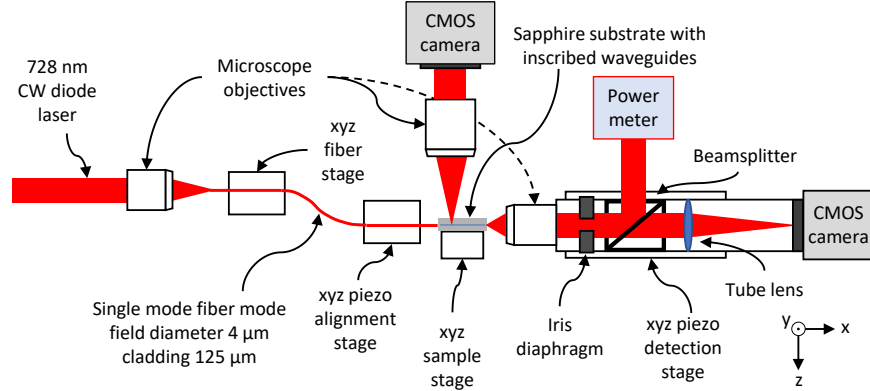


Figure 4: Schematic representation of the waveguide characterization setup. Laser light from a 728 nm diode laser is coupled into a single mode fiber via a microscope objective. This fiber is fixed on a xyz-Piezo stage for alignment to the sample. A microscope images the fiber tip and incoupling site of the sample from above. The outgoing light from the sample is collected by a horizontal microscope mounted on a xyz-Piezo stage. It allows image capture via a CMOS camera as well as power measurement via a power meter.

tion. The mode profile gives information on the confinement properties of the waveguide, allowing to discriminate between single and multimode behavior. Ideally, waveguides presenting circular mode profiles with near-Gaussian intensity distributions are preferred, as single mode operation is crucial for the vast majority of integrated optical applications, since it avoids inter-modal power transfers and allows a proper engineering of waveguide coupling.

A measurement setup for optical waveguide analysis includes a light source that is coupled into the waveguide under test. The light is then guided through the waveguide and exits at the other end. The output light is detected using a microscope to observe the waveguide mode profile as well as with a powermeter to measure the transmitted power.

Fig. 4 shows a sketch of the measurement setup for optical waveguide analysis. Laser light from a 728 nm laser diode (Cobolt 06-MLD) is end-fire coupled by means of a microscope objective into a single-mode fiber (Thorlabs 630HP) placed on an xyz-stage for manual adjustment. The other end of the fiber is stripped and cleaved; the bare fiber tip is brought as close as possible to the waveguide end facet on the sidewall of the sapphire sample. Consequently, the light from the bare single mode fiber is butt-coupled into the inscribed waveguides in the sapphire substrate placed on a xyz-stage for adjustment. An additional video microscope provides a top view of the fiber-waveguide interface to facilitate the adjustment. The output light on the opposite end of the wave-

uide in the sapphire substrate is collected using a microscope objective with a numerical aperture of 0.5. Stray light is minimized by an iris diaphragm and a beam-splitter divides the beam into two ports. The first beam is measured by a powermeter to determine the waveguide losses. The second beam is steered onto a CMOS camera to image the mode profile of the light propagating along the waveguide. To optimize the positioning of fiber-butt-coupling as well as the collecting objective unit, including the power meter and the CMOS camera, three-axis ultra-high resolution piezo actuators (Newport NanoPZ), allowing a minimum incremental motion of 30 nm, are used. For determining the losses, the power of the light directly emitted from the fiber is measured as a reference and set into relation to the output power of the sapphire waveguide when coupled to the fiber. This yields the total loss of the waveguide, which accounts for the coupling losses at input and output ports of the waveguide and for the propagation loss along the waveguide.

4 Results and Discussion

4.1 Waveguide geometry optimization

Circular depressed cladding structures were inscribed in sapphire by positioning multiple laser tracks along a ring-shaped pattern. Positioning the stages in a circular pattern results in an elliptically shaped waveguide in sapphire due to the different refraction with varying writing depth. Therefore, elliptically positioning patterns were investigated to compensate the ellipticity of the resulting waveguide. The ellipticity factor is defined as the ratio between minor (vertical) axis and major (horizontal) axis of the written pattern and was investigated from 1 down to 0.45. No measurable deviations of the total losses were found over the entire range. Optimizing the waveguide geometry involved adjusting physical characteristics, such as dimensions and shape of the waveguides, in particular the number of lines and the diameter of laser-inscribed ring-shaped pattern, as well as optimizing laser parameters: laser pulse energy, laser repetition rate or laser scanning speed. The optimization process was repeated with single-mode profile and lowest total loss as targets. Waveguides were written with fs-laser light at 524 nm with a polarization along the x-direction. For focusing into the sapphire volume, a microscope objective with a numerical aperture of 0.75 was used, resulting in elliptical cross sections of single written lines with an estimated aspect ratio of 2.3. The writing velocity was set to 15 mm/s. The pulse duration, pulse energy and repetition rate were set to 300 fs, 65 or 78 nJ and 100 kHz, respectively. The investigated waveguides were typically 1 cm long except for the cut-back measurements.

The depressed cladding geometry was varied in different aspects. First, the number of lines that make up a ring-shaped cladding pattern with a radius of 5 μm was varied from 3 to 30 lines. Fig. 5 shows the measured total loss depending on the number of lines written with laser pulse energies of 65 nJ (blue) and 78 nJ (orange). Claddings consisting of less than 10 lines did not show any

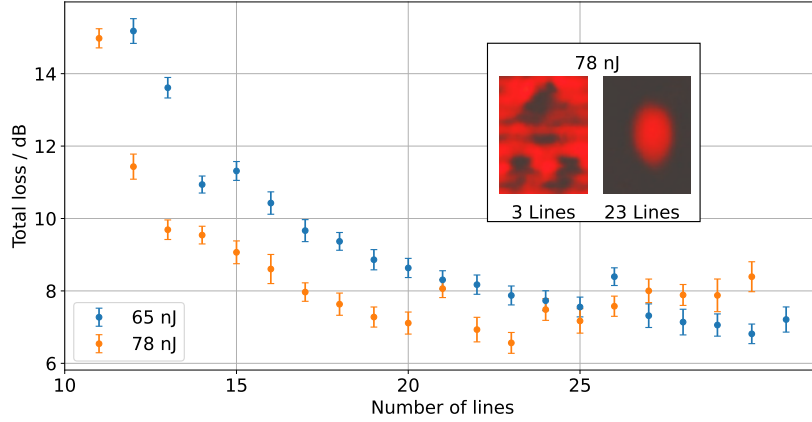


Figure 5: Total loss as a function of the number of lines written forming the depressed cladding with laser pulse energies of 65 nJ (blue) and 78 nJ (orange). Claddings with less than 10 lines did not show any wave-guiding properties. Inset: Mode profile images for claddings written with 78 nJ and consisting of 3 lines and 23 lines. Total loss was 15.2(3) dB and 6.5(2) dB for 12 and 23 lines, respectively.

wave-guiding behavior, compare the profile of the waveguide with three lines in contrast to the Gaussian mode profile of the waveguide with 23 lines in the inset Fig. 5. The measured total loss is highest for claddings consisting of 11 lines and decreases rapidly with increasing amount of lines, reaching a minimum of 6.6(2) dB at 23 lines for a pulse energy of 78 nJ and 6.8(2) dB at 30 lines for a pulse energy of 65 nJ. For a cladding consisting of 21 lines, the distance between lines is 1.5 μm at the given radius of 5 μm . This distance between the lines was maintained for all further waveguides.

Table 1 displays waveguides with different core radii of 4 – 15 μm fabricated again with pulse energies of 65 and 78 nJ. On the top, exemplary microscope images of the DCW ends are shown, while on bottom the corresponding mode profiles are shown and total loss are indicated. For waveguides with lines in a radius of 4 μm , no light guiding is observed. For radii from 4.5 μm to 7.5 μm , mode profiles reveal a near Gaussian shape robust against slight misalignments, indicating single mode wave-guiding. For a core radius of 10 μm and more, the images adopt more complex structures changing with the alignment of the end-fire coupled single mode fiber, indicating multi-mode behavior. Hereafter, the core radius is kept constant at 7.5 μm showing the lowest total loss of 8.6(2) dB and 8.3(2) dB at a pulse energy of 65 nJ and 78 nJ, respectively, while maintaining single-mode guiding.

| Radius/ μm | 4 | 4.5 | 5 | 7.5 | 10 | 12.5 | 15 |
|-----------------------|---|------|------|-----|-----|------|-----|
| 65 nJ | | | | | | | |
| | | | | | | | |
| Total loss/dB | | 17.0 | 16.0 | 8.6 | 6.6 | 6.1 | 5.8 |
| 78 nJ | | | | | | | |
| | | | | | | | |
| Total loss/dB | | 14.4 | 12.9 | 8.3 | 6.4 | 5.6 | 5.1 |

Table 1: Microscope images (top, brown backdrop) and near-field images (bottom, black backdrop) of DCWs written with varying radii (4 - 15 μm) at pulse energies of 65 nJ and 78 nJ. The black scale bar depicts 10 μm . The numbers at the bottom of each figure indicate the total loss for a 10 mm long waveguide.

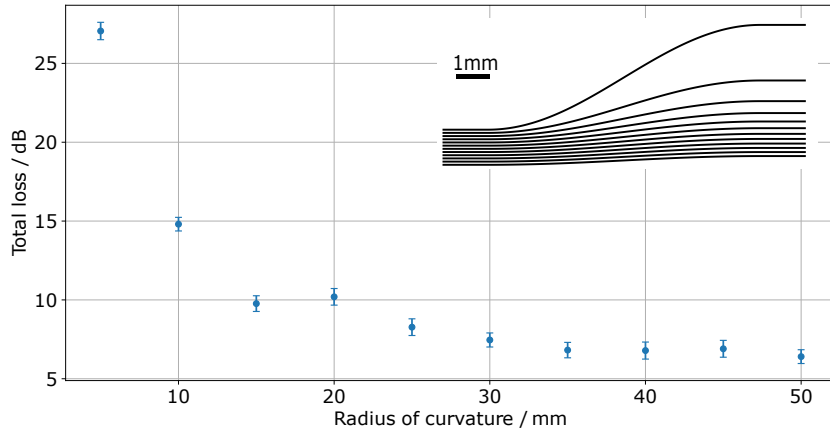


Figure 6: Total loss of waveguides depending on their radius of curvature. Inset: Top view of curves as drawn in the CAD program. Curvature radius of 5 mm (highest curvature, top) to 60 mm (lowest curvature, bottom). Waveguides were written with an ellipticity factor of 0.6 in the CAD program resulting in a circular pattern in Sapphire at a pulse energy of 65 nJ.

4.2 Curved depressed cladding waveguides

To investigate the influence of the radius of curvature on the waveguide propagation characteristics, s-shaped curved waveguides with variable radii of curvature were fabricated and measured. S-bend curves were written with curvature radii from 5 mm to 60 mm across a sample length of 1 cm and a pulse energy of 65 nJ was used. Note that with a lower radius of curvature, the horizontal offset in y-direction between input and output and the total length of the waveguide are increased.

Fig. 6 shows the total loss as function of the radius of curvature of the waveguide. With radii of curvature above 35 mm, the total loss is in the interval given by two standard deviations of measurements of straight waveguides. The total loss starts to increase with radii of curvature increasing from 15 mm to 35 mm and a rapid increase is observed for radii smaller than 15 mm.

4.3 Propagation loss

All loss values reported so far concern the total loss. The total loss can be broken down into three components: in-coupling loss, propagation loss, and out-coupling loss. In-coupling loss refers to the amount of light that is lost as it is coupled into the waveguide. This loss can occur due to Fresnel reflection at the sample surface or due to an imperfect match between the waveguide mode and the light source's mode. Propagation loss refers to the amount of light that is lost as it propagates through the waveguide. This loss can occur due to absorption or scattering induced at material defects. Out-coupling loss

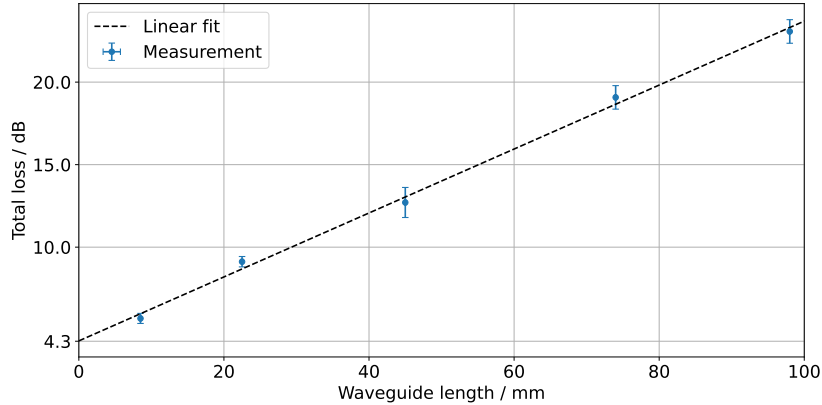


Figure 7: Measured total loss in dependence of the waveguide length. The error of the waveguide length is ± 0.1 mm and is smaller than the marker size. The linear fit (dashed line) gives waveguide propagation loss of $1.9(3)$ dB/cm and in- and out-coupling losses of $4.3(3)$ dB.

refers to the amount of light that is lost as it exits the waveguide and is largely determined by the Fresnel loss, as the characterization setup aims to collect the entire light field after the waveguide.

In general, the optimization of the waveguide geometry is done to minimize these losses. The in-coupling and out-coupling losses can be reduced by properly aligning the light source and detector with the waveguide, and by using mode-matching techniques. The propagation loss can be reduced by using a low-loss waveguide material, by designing the waveguide to have a small mode area, and by optimizing fs-laser writing parameters for writing tracks with low absorption and scattering cross sections.

To determine the contribution of the propagation loss, five identical straight waveguides (ring-shaped cladding pattern with a radius of $5 \mu\text{m}$) were written in a sapphire sample with a length of 100 mm. The length of the sample was gradually decreased by scribing, breaking and subsequent grinding and polishing. The length error is ± 0.1 mm and results from the uncertainty in grinding and polishing-depth, after the breaking process. After each breaking step, the total loss was measured for each of the five waveguides to perform a so-called cutback measurement.

Fig. 7 shows the measured total loss in dependence of the sample length. The offset of the linear fit on the y-axis corresponds to the constant in- and out-coupling losses of $4.3(3)$ dB, while its slope equals the propagation loss, which amounts to $1.9(3)$ dB/cm for the presented waveguides at the applied wavelength of 728 nm.

5 Conclusion and Outlook

To the best of our knowledge, we demonstrated the first fs-laser writing of depressed cladding waveguides in sapphire for the visible wavelength range, and of curved waveguides in undoped sapphire. The use of a fs laser allows for precise control over the waveguide geometry and the ability to create highly localized modifications of refractive index in the bulk material, resulting in highly customizable waveguides by adjusting various structural and laser parameters. We achieved transmission losses of 1.9(3) dB/cm at $\lambda = 728$ nm and coupling losses of 4.3(3) dB. These values allow the realization of single-qubit and multi-qubit quantum gates with Calcium ions as shown with planar-fabricated integrated optics with similar values in [30]. With advancements in laser technology and optimization techniques, it is expected that the quality of the presented waveguides will continue to improve and that depressed cladding waveguides can also be used for ionization, cooling, and repumping of trapped ions. The use of sapphire as a waveguide material offers several advantages such as its high thermal conductivity, high mechanical strength and chemical stability, which are important for many applications including trapped ion quantum computing and sensing.

6 Funding

Austrian Research Promotion Agency (FFG), project “OptoQuant” (37798980)

7 Disclosures

The authors declare no conflicts of interest.

8 Data availability

Data underlying the results presented in this paper are not publicly available at this time but may be obtained from the authors upon reasonable request.

References

- [1] H. Häffner, C. Roos, and R. Blatt. Quantum computing with trapped ions. *Physics Reports*, 469(4):155–203, dec 2008.
- [2] Colin D. Bruzewicz, John Chiaverini, Robert McConnell, and Jeremy M. Sage. Trapped-ion quantum computing: Progress and challenges. *Applied Physics Reviews*, 6(2):021314, jun 2019.
- [3] R. Blatt and C. F. Roos. Quantum simulations with trapped ions. *Nature Physics*, 8(4):277–284, apr 2012.

- [4] M. Brewer, J.-S. Chen, A. M. Hankin, E. R. Clements, C. W. Chou, D. J. Wineland, D. B. Hume, and D. R. Leibbrandt. Al⁺ quantum logic clock with a systematic uncertainty below 1e-18. *Physical Review Letters*, 123(3):033201, jul 2019.
- [5] Karan K. Mehta, Colin D. Bruzewicz, Robert McConnell, Rajeev J. Ram, Jeremy M. Sage, and John Chiaverini. Integrated optical addressing of an ion qubit. *Nature Nanotechnology*, 11(12):1066–1070, aug 2016.
- [6] Matthew L Day, Kaushal Choonee, Zachary Chaboyer, Simon Gross, Michael J Withford, Alastair G Sinclair, and Graham D Marshall. A micro-optical module for multi-wavelength addressing of trapped ions. *Quantum Science and Technology*, 6(2):024007, feb 2021.
- [7] Hayden McGuinness, Michael Gehl, Craig Hogle, William J. Setzer, Nickolas Karl, Nicholas Jaber, Justin Schultz, Joonhyuk Kwon, Megan Ivory, Rex Kay, Daniel Dominguez, Douglass Trotter, Matt Eichenfield, and Daniel L. Stick. Integrated photonics for trapped ion quantum information experiments at sandia national laboratories. In Mario Agio, Igor Aharonovich, Cesare Soci, and Matthew T. Sheldon, editors, *Quantum Nanophotonic Materials, Devices, and Systems 2022*. SPIE, oct 2022.
- [8] R. J. Niffenegger, J. Stuart, C. Sorace-Agaskar, D. Kharas, S. Bramhavar, C. D. Bruzewicz, W. Loh, R. T. Maxson, R. McConnell, D. Reens, G. N. West, J. M. Sage, and J. Chiaverini. Integrated multi-wavelength control of an ion qubit. *Nature*, 586(7830):538–542, oct 2020.
- [9] Alfredo Ricci Vasquez, Carmelo Mordini, Chloé Vernière, Martin Stadler, Maciej Malinowski, Chi Zhang, Daniel Kienzler, Karan K. Mehta, and Jonathan P. Home. Control of an atomic quadrupole transition in a phase-stable standing wave. *Physical Review Letters*, 130(13):133201, mar 2023.
- [10] K. Miura, Jianrong Qiu, H. Inouye, T. Mitsuyu, and K. Hirao. Photowritten optical waveguides in various glasses with ultrashort pulse laser. *Applied Physics Letters*, 71(23):3329–3331, dec 1997.
- [11] Roberto Osellame, Giulio Cerullo, and Roberta Ramponi, editors. *Femtosecond Laser Micromachining*. Springer Berlin Heidelberg, 2012.
- [12] Dezhi Tan, Zhuo Wang, Beibei Xu, and Jianrong Qiu. Photonic circuits written by femtosecond laser in glass: improved fabrication and recent progress in photonic devices. *Advanced Photonics*, 3(02), mar 2021.
- [13] Bangshan Sun, Fyodor Morozko, Patrick S. Salter, Simon Moser, Zhikai Pong, Raj B. Patel, Ian A. Walmsley, Mohan Wang, Adir Hazan, Nicolas Barré, Alexander Jesacher, Julian Fells, Chao He, Aviad Katiyi, Zhen-Nan Tian, Alina Karabchevsky, and Martin J. Booth. On-chip beam rotators, adiabatic mode converters, and waveplates through low-loss waveguides with variable cross-sections. *Light: Science & Applications*, 11(1), jul 2022.

- [14] Giacomo Corrielli, Andrea Crespi, and Roberto Osellame. Femtosecond laser micromachining for integrated quantum photonics. *Nanophotonics*, 10(15):3789–3812, oct 2021.
- [15] Ming-Ming Dong, Cheng-Wei Wang, Zheng-Xiang Wu, Yang Zhang, Huai-Hai Pan, and Quan-Zhong Zhao. Waveguides fabricated by femtosecond laser exploiting both depressed cladding and stress-induced guiding core. *Optics Express*, 21(13):15522, jun 2013.
- [16] Yingying Ren, Yang Jiao, Javier R. Vázquez de Aldana, and Feng Chen. Ti:sapphire micro-structures by femtosecond laser inscription: Guiding and luminescence properties. *Optical Materials*, 58:61–66, aug 2016.
- [17] Jean-Philippe Bérubé, Jerome Lapointe, Albert Dupont, Martin Bernier, and Réal Vallée. Femtosecond laser inscription of depressed cladding single-mode mid-infrared waveguides in sapphire. *Opt. Lett.*, 44(1):37, dec 2018.
- [18] Carolina Romero, Javier García Ajates, Feng Chen, and Javier R. Vázquez de Aldana. Fabrication of tapered circular depressed-cladding waveguides in nd:YAG crystal by femtosecond-laser direct inscription. *Micromachines*, 11(1):10, dec 2019.
- [19] Lingqi Li, Weijin Kong, and Feng Chen. Femtosecond laser-inscribed optical waveguides in dielectric crystals: a concise review and recent advances. *Advanced Photonics*, 4(02), mar 2022.
- [20] Feng Chen and J. R. Vázquez de Aldana. Optical waveguides in crystalline dielectric materials produced by femtosecond-laser micromachining. *Laser & Photonics Reviews*, 8(2):251–275, may 2013.
- [21] Cornelius Hempel. *Digital quantum simulation, Schrödinger cat state spectroscopy and setting up a linear ion trap*. PhD thesis, University of Innsbruck, 2014.
- [22] M Hellwig, A Bautista-Salvador, K Singer, G Werth, and F Schmidt-Kaler. Fabrication of a planar micro penning trap and numerical investigations of versatile ion positioning protocols. *New Journal of Physics*, 12(6):065019, June 2010.
- [23] N Daniilidis, S Narayanan, S A Möller, R Clark, T E Lee, P J Leek, A Wallraff, St Schulz, F Schmidt-Kaler, and H Häffner. Fabrication and heating rate study of microscopic surface electrode ion traps. *New Journal of Physics*, 13(1):013032, jan 2011.
- [24] D. T. C. Allcock, T. P. Harty, C. J. Ballance, B. C. Keitch, N. M. Linke, D. N. Stacey, and D. M. Lucas. A microfabricated ion trap with integrated microwave circuitry. *Applied Physics Letters*, 102(4):044103, jan 2013.

- [25] P. J. Kunert, D. Georgen, L. Bogunia, M. T. Baig, M. A. Baggash, M. Johanning, and Ch. Wunderlich. A planar ion trap chip with integrated structures for an adjustable magnetic field gradient. *Applied Physics B*, 114(1–2):27–36, December 2013.
- [26] Yuechen Jia, Shixiang Wang, and Feng Chen. Femtosecond laser direct writing of flexibly configured waveguide geometries in optical crystals: fabrication and application. *Opto-Electronic Advances*, 3(10):190042–190042, 2020.
- [27] Jing Bai, Guanghua Cheng, Xuewen Long, Yishan Wang, Wei Zhao, Guofu Chen, Razvan Stoian, and Rongqing Hui. Polarization behavior of femtosecond laser written optical waveguides in ti:sapphire. *Optics Express*, 20(14):15035, jun 2012.
- [28] Mohan Wang, Patrick S. Salter, Frank P. Payne, Adrian Shipley, Stephen M. Morris, Martin J. Booth, and Julian A. J. Fells. Single-mode sapphire fiber bragg grating. *Optics Express*, 30(9):15482, apr 2022.
- [29] Stefan Kefer, Gian-Luca Roth, Julian Zettl, Bernhard Schmauss, and Ralf Hellmann. Sapphire photonic crystal waveguides with integrated bragg grating structure. *Photonics*, 9(4):234, apr 2022.
- [30] Karan K. Mehta, Chi Zhang, Maciej Malinowski, Thanh-Long Nguyen, Martin Stadler, and Jonathan P. Home. Integrated optical multi-ion quantum logic. *Nature*, 586(7830):533–537, oct 2020.